PLANT SCIENCE

Phosphoenolpyruvate reallocation links nitrogen fixation rates to root nodule energy state

Xiaolong Ke[1,2,3], Han Xiao[1,2,3], Yaqi Peng[1,2,3], Jing Wang[1], Qi Lv[1,2], Xuelu Wang[1,2,3]*

Legume-rhizobium symbiosis in root nodules fixes nitrogen to satisfy the plant's nitrogen demands. The nodules' demand for energy is thought to determine nitrogen fixation rates. How this energy state is sensed to modulate nitrogen fixation is unknown. Here, we identified two soybean (*Glycine max*) cystathionine β-synthase domain–containing proteins, nodule AMP sensor 1 (GmNAS1) and NAS1-associated protein 1 (GmNAP1). In the high–nodule energy state, GmNAS1 and GmNAP1 form homodimers that interact with the nuclear factor-Y C (NF-YC) subunit (GmNFYC10a) on mitochondria and reduce its nuclear accumulation. Less nuclear GmNFYC10a leads to lower expression of glycolytic genes involved in pyruvate production, which modulates phosphoenolpyruvate allocation to favor nitrogen fixation. Insight into these pathways may help in the design of leguminous crops that have improved carbon use, nitrogen fixation, and growth.

Legumes have evolved specialized nitrogen-fixing organs called root nodules by establishing symbiotic relationships with rhizobia, which require a large amount of extra energy for nitrogen fixation. The symbiotic nodules obtain photoassimilates (mainly sucrose) and metabolize them through glycolysis to produce phosphoenolpyruvate (*1*–*3*). Phosphoenolpyruvate is converted into either malate to fuel atmospheric nitrogen fixation in bacteroids or pyruvate for adenosine triphosphate (ATP) production in mitochondria for nitrogen assimilation and other cellular activities (fig. S1), and its allocation likely regulates nodule nitrogen fixation capacity (*4*–*10*). Soybean (*Glycine max*) nodule nitrogen fixation capacity is low under anaerobic or phosphorus-deficient conditions but increases when the supply of oxygen or phosphorus increases as the nodule energy state changes (*11*, *12*). As the nodule energy state decreases after transfer to darkness or high nitrate supply, leguminous nodule nitrogen fixation capacity also decreases (*13*–*16*). Given the high energy needs of symbiotic nitrogen fixation, it is likely that nodule energy-state changes regulate nodule nitrogen fixation capacity. How nodule energy state is sensed and how the information regulates nodule nitrogen fixation capacity has been unclear.

Cystathionine β-synthase (CBS) domains are conserved protein modules that can bind adenosyl compounds, such as adenosine monophosphate (AMP), adenosine diphosphate (ADP), ATP, and *S*-adenosyl methionine, to regulate biological processes by associating with other functional regions of CBS domain–containing proteins (CDCPs) (*17*–*21*). AMP-activated protein kinases, with α, β, and γ subunits, sense cellular energy status and respond to low-energy stress in mammalian cells (*22*, *23*). The greater AMP concentration associated with low–cellular energy states can enhance AMP binding to the CBS domains of the γ subunit of AMP-activated protein kinases to allosterically activate its catalytic α subunit, thereby initiating downstream signaling to maintain cellular energy homeostasis (*18*, *19*). CBSX proteins contain a pair of CBS domains, bind to AMP, and activate thioredoxins in different organelles to maintain cellular redox homeostasis in *Arabidopsis* (*Arabidopsis thaliana*) (*24*), suggesting a role for CDCPs in plant cellular energy sensing.

GmNAS1 and GmNAP1 sense nodule energy state to regulate nodule nitrogen fixation capacity

To identify CDCPs that might sense nodule energy state in soybean, we examined the expression patterns of 71 soybean *CDCP* genes using Soybean eFP Browser (*25*, *26*). We found that the CDCP gene *GmCBS22* was highly expressed in nodules, flowers, and leaves, whereas its close homolog *GmCBS14* was specifically expressed only in root nodules (fig. S2A). *GmCBS22* and *GmCBS14* are highly expressed in mature nodules, with *GmCBS22* showing a broad expression and *GmCBS14* expressed specifically in the nodule infection zone and vascular bundles (fig. S2, B to N). Knockdown of *GmCBS22* and *GmCBS14* in hairy roots decreased nodule nitrogenase activity by about 50%, whereas nodule number and weight were unaffected (fig. S3, A and B), indicating that *GmCBS22* and *GmCBS14* may regulate nodule nitrogen fixation.

GmCBS22 and *GmCBS14* are predicted to encode proteins with an N-terminal chloroplast transit peptide (cTP), four tandem CBS domains, a Phox and Bem1 (PB1) domain, and a C-terminal transmembrane region (TMR) (Fig. 1A and fig. S4, A and B). We expressed cTP-GFP-GmCBS22 [GmCBS22 fused to green fluorescent protein (GFP) after the cTP] or GmCBS14-GFP-TMR (GmCBS14 fused to GFP before the TMR) in *Nicotiana benthamiana* leaf epidermal cells and soybean nodules and observed localization to mitochondria (Fig. 1B and fig. S4C), which was further confirmed by subcellular fractionation (fig. S4D). When the C-terminal TMR was conformationally obscured by cyan fluorescent protein (CFP) in GmCBS22-CFP and GmCBS14-CFP fusion proteins, CFP fluorescence accumulated in the nucleus and the cytoplasm (fig. S4E), indicating that the C-terminal TMR is required for mitochondrial localization of GmCBS22 and GmCBS14. We noticed occasional ring fluorescence patterns for cTP-GFP-GmCBS22 and GmCBS14-GFP-TMR in *N. benthamiana* leaf epidermal cells, suggesting their localization to the mitochondrial outer membrane (fig. S4F) (*27*).

We then tested the ability of GmCBS22 and GmCBS14 proteins to bind various adenylates and found that one GmCBS22 molecule can bind one AMP with a dissociation constant (K_d) of 3.94 μM and ADP with a K_d of 40.32 μM (Fig. 1, C and D), whereas ATP and cyclic AMP (cAMP) did not bind to GmCBS22 (fig. S5A). By contrast, GmCBS14 did not bind to any of the tested adenylates (fig. S5B). Deletion of any of the four CBS domains in GmCBS22 abolished its AMP binding ability (fig. S6, A to D). The secondary structures of GmCBS22 and GmCBS14 were unaffected by the addition of AMP, ADP, ATP, or cAMP (fig. S7, A and B). Like many other CDCPs (*21*), GmCBS22 and GmCBS14 formed homodimers and heterodimers (Fig. 1E and fig. S8). Recombinant His-GmCBS22 lacking any CBS domain still interacted with GmCBS22 and GmCBS14 tagged with glutathione *S*-transferase (GST) (fig. S9A), whereas deletion of the PB1 domain of GmCBS22 eliminated the homodimerization of GmCBS22 and heterodimerization of GmCBS22 and GmCBS14, and deletion of the PB1 domain of GmCBS14 also eliminated the homodimerization of GmCBS14 and heterodimerization of GmCBS22 and GmCBS14 (fig. S9B). Moreover, the addition of AMP enhanced formation of GmCBS22-GmCBS14 heterodimers but blocked formation of GmCBS22 homodimers (Fig. 1E and fig. S8B). Therefore, GmCBS22 and GmCBS14 may function as energy sensors in soybean nodules by directly binding to AMP and forming dynamic dimers on the mitochondrial membrane. We therefore renamed GmCBS22 as soybean nodule AMP sensor 1 (GmNAS1) and GmCBS14 as NAS1-associated protein 1 (GmNAP1).

Under our growth conditions, sucrose treatment, which significantly increased nodule energy state (Fig. 1F), can enhance nodule nitrogenase activity in soybean "Williams 82" (W82) plants (Fig. 1G). To investigate whether

[1]State Key Laboratory of Crop Stress Adaptation and Improvement, School of Life Sciences, Henan University, Zhengzhou 450046, China. [2]The Academy for Advanced Interdisplinary Studies, Henan University, Zhengzhou 450046, Henan, China. [3]Sanya Institute of Henan University, Sanya 572025, Hainan, China.
*Corresponding author. Email: xueluw@henu.edu.cn

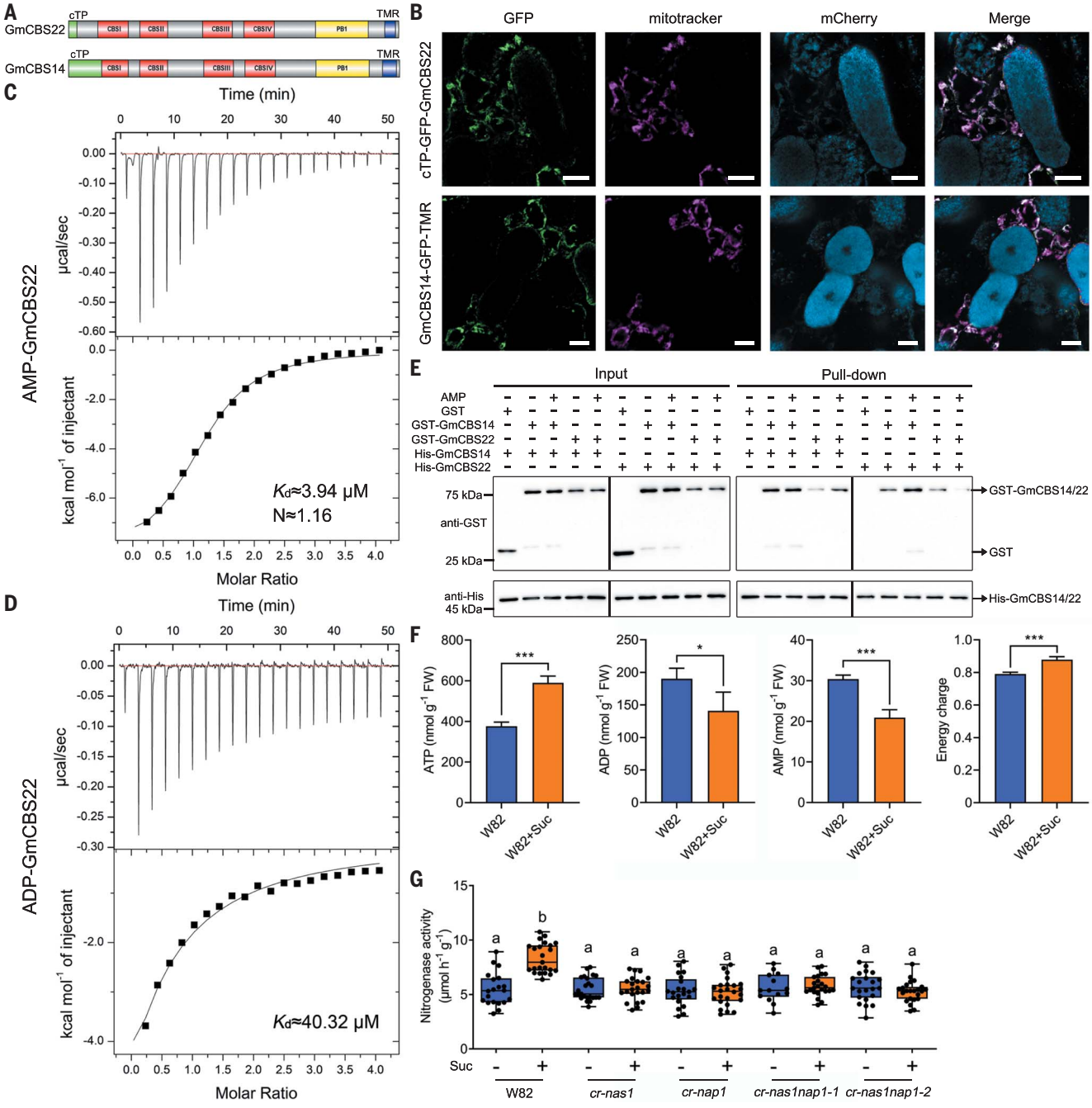

Fig. 1. GmNAS1 and GmNAP1 are nodule energy sensors that regulate the response of nodule nitrogen fixation capacity to nodule energy state. (**A**) Schematic diagram of the GmCBS22 and GmCBS14 proteins. (**B**) GmCBS22 and GmCBS14 localization in nodule cells. Nodules of *pGmCBS22:cTP-GFP-GmCBS22* and *pGmCBS14:GmCBS14-GFP-TMR* transgenic hairy roots were sectioned to observe GFP fluorescence. Mitotracker was used to stain mitochondria; mCherry indicates infected cells containing the strain USDA110-mCherry. Scale bars are 20 μm. (**C** and **D**) Isothermal titration calorimetry analysis of GmCBS22 binding to AMP (C) or ADP (D). The black lines (bottom) are the best fit to the one-site model. (**E**) Pull-down assays of His-GmCBS22, His-GmCBS14, GST-GmCBS22, and GST-GmCBS14. The experiment was performed three times with comparable results. (**F**) Changes in ATP, ADP, and AMP contents and energy charge of W82 nodules after sucrose treatment. Data are means ± SD of four biological replicates. FW, fresh weight. (**G**) Nodule nitrogenase activity of W82 and *GmNAS1* and *GmNAP1* mutants without and with sucrose treatment. Boxes represent the first quartile, median, and third quartile, and whiskers represent minimum and maximum values. Significant differences were determined by Student's *t* test (**P* < 0.05, and ****P* < 0.001) in (F) or by one-way analysis of variance (ANOVA) and post hoc Tukey's test, with different lowercase letters indicating significant differences (*P* < 0.05) in (G).

GmNAS1 and GmNAP1 can sense nodule energy state to regulate nodule nitrogen fixation capacity, we created knockout mutants of *GmNAS1* and *GmNAP1*, namely, *cr-nas1*, *cr-nap1*, *cr-nas1nap1-1*, and *cr-nas1nap1-2* (fig. S10, A and B). Under our growth conditions, these mutants showed similar nodule number, weight, and nitrogenase activity relative to the wild type (Fig. 1G and fig. S10C). However, although the nodule energy state of these mutants was similar to that of the wild type (fig. S11, A to D), sucrose treatment failed to

enhance nodule nitrogen fixation capacity in all the mutants (Fig. 1G), indicating that *GmNAS1* and *GmNAP1* mediate the linkage between nitrogen fixation capacity and nodule energy state (fig. S11, E to I). Changes in light intensity affected photosynthesis, nodule energy state, and nitrogen fixation capacity (fig. S12, A to F). Knockout of *GmNAS1* and *GmNAP1* also eliminated the increase in nodule nitrogen fixation capacity that follows enhanced light intensity (fig. S12F). Together, these results show that GmNAS1 and GmNAP1 are needed for nodule nitrogen fixation capacity to respond to changes in nodule energy state.

GmNAS1 and GmNAP1 regulate GmNFYC10a nuclear localization

To elucidate how GmNAS1 and GmNAP1 regulate nodule nitrogen fixation capacity in response to nodule energy state, we conducted co-immunoprecipitation (co-IP) assays followed by tandem mass spectrometry (MS/MS). We identified additional GmNAP1 interactors, including a nuclear factor-Y C (NF-YC) subunit, GmNFYC10a (fig. S13, A and B, and data S1). Considering the role of NF-YC subunits in symbiotic nitrogen fixation (*28*, *29*), we tested and confirmed the interaction of GmNAS1 and GmNAP1 with GmNFYC10a (Fig. 2, A and B). The addition of AMP largely blocked the interaction between GmNAS1 and GmNFYC10a but not that between GmNAP1 and GmNFYC10a (Fig. 2B). GmNAS1 lacking any CBS domain still interacted with GmNFYC10a, and the addition of AMP hardly affected their interaction (fig. S14A). Given that AMP impaired GmNAS1 homodimerization (Fig. 1E), we hypothesized that GmNAS1 or GmNAP1 homodimerization is required for their interaction with GmNFYC10a. Indeed, GmNAS1 and GmNAP1 lacking the PB1 domain failed to interact with GmNFYC10a (fig. S14B). Moreover, AMP-promoted GmNAS1-GmNAP1 heterodimerization (Fig. 1E and fig. S8B) also facilitated the dissociation of GmNAP1 homodimers and inhibited its interaction with GmNFYC10a (Fig. 2C). Interaction of GmNAS1 and GmNAP1 with GmNFYC10a was inhibited by AMP (Fig. 2D) but enhanced by sucrose in vivo (fig. S15).

Unlike the fluorescence that was mainly observed on mitochondria during bimolecular fluorescence complementation (BiFC) assays of GmNFYC10a and GmNAS1 and GmNAP1 (Fig. 2A), GmNFYC10a-GFP only localized to the nucleus (Fig. 2E), suggesting that GmNFYC10a is proximal to mitochondria through its interaction with GmNAS1 and GmNAP1. Because higher AMP levels can weaken the interaction of GmNAS1 and GmNAP1 with GmNFYC10a (Fig. 2, B to D), we hypothesized that a low–nodule energy state may enhance GmNFYC10a translocation from mitochondria to nuclei. Indeed, oligomycin, an inhibitor of mitochondrial ATP synthase, or AMP treatment significantly promoted the nuclear accumulation of GmNFYC10a-GFP in nodule cells (Fig. 2F). More GmNFYC10a-GFP localized to the cytoplasm in the *cr-nas1* and *cr-nap1* nodules than in W82 nodules under mock conditions (Fig. 2F and fig. S16, A and B), confirming that GmNAS1 and GmNAP1 maintain GmNFYC10a localization to mitochondria. Oligomycin or AMP treatment promoted GmNFYC10a-GFP nuclear localization in *cr-nap1* but not in *cr-nas1* mutants (fig. S16, A and B), suggesting that GmNAS1 but not GmNAP1 can primarily respond to increased AMP to enhance GmNFYC10a nuclear accumulation. GmNFYC10a-GFP accumulated in the cytoplasm and nucleus in most nodule cells of the *cr-nas1nap1-2* mutant, regardless of whether they were treated with oligomycin or AMP (fig. S16C). Taken together, these results demonstrate that GmNAS1 and GmNAP1 regulate the GmNFYC10a nuclear accumulation in response to changing nodule energy state.

GmNFYC10 regulates glycolysis for pyruvate production

We then created the knockout mutant *cr-nfyc10* through genome editing (fig. S17A) as well as *gGmNFYC10a-Flag* overexpression plants and found that neither showed changes in nodule number, weight, or nitrogenase activity relative to the wild type under normal growth conditions (Fig. 3, A and B, and fig. S17, B to D). However, unlike the wild type, the *cr-nfyc10* and *gGmNFYC10a-Flag* plants did not show the sucrose-enhanced nodule nitrogen fixation capacity (Fig. 3, A and B), indicating that the proper expression level of *GmNFYC10* is required for efficient nitrogen fixation under the high–nodule energy state.

To explore how the GmNAS1-GmNAP1-GmNFYC10 module regulates nodule nitrogen fixation capacity, we conducted RNA sequencing (RNA-seq) analysis of *Ri-GmNAS1-NAP1* (*Ri-GmCBS22-14*) nodules (Fig. 3, C and D). Kyoto Encyclopedia of Genes and Genomes (KEGG) analysis (*30*) of the down-regulated genes showed a variety of biological processes regulated by *GmNAS1* and *GmNAP1* (Fig. 3E). Considering the pivotal role of glycolysis in nodule energy supply (fig. S1) (*1*–*3*), we analyzed 26 down-regulated genes involved in the glycolysis-gluconeogenesis pathway (data S2). Ten glycolytic genes among these genes contain five encoding pyruvate kinases (PKs) (Fig. 3F and fig. S18, A and B). Expression of enolase genes in glycolysis was not down-regulated in *Ri-GmNAS1-NAP1* nodules (fig. S18C). Promoter analysis of 10 down-regulated glycolytic genes revealed a CCAAT element, the binding site of the NF-Y transcriptional complex (fig. S19A) (*31*). Furthermore, we determined that GmNFYC10a binds to the *PK1a*, *GAPC1*, and *PK2a* promoters and activates their expression (Fig. 3, G and H). Expression of most glycolytic genes was down-regulated in *cr-nfyc10* nodules (fig. S19B). Expression of several glycolytic genes was reduced in the *Ri-GmNFYC10* nodules (fig. S19, C and D), whereas expression of most glycolytic genes was higher in the *gGmNFYC10a-Flag* nodules (fig. S19, E and F). Given that half of the regulated glycolytic genes encode PKs (Fig. 3F), we examined pyruvate contents in *Ri-GmNFYC10* and *gGmNFYC10a-Flag* nodules. Compared with wild type nodules, pyruvate contents were about 40% lower in the *Ri-GmNFYC10* nodules and 50% higher in the *gGmNFYC10a-Flag* nodules (fig. S19G). Knockdown of *PK1*, *GAPC1*, or *PK2* decreased nodule nitrogenase activity without affecting nodule number or weight (fig. S20, A and B). Together, these findings indicate that GmNFYC10, regulated by GmNAS1 and GmNAP1, can activate glycolysis for pyruvate production in soybean nodules.

The GmNAS1-GmNAP1-GmNFYC10 module regulates PEP allocation in nodules

Because a reduced nodule energy state can promote GmNFYC10a nuclear accumulation (Fig. 2F), we determined that sucrose treatment leads to diminished nuclear accumulation and enhanced mitochondrial localization of GmNFYC10a (Fig. 4A). Expression levels of the glycolytic genes activated by GmNFYC10 were also down-regulated after sucrose treatment (Fig. 4B), which did not happen in the *cr-nas1*, *cr-nap1*, *cr-nas1nap1-1*, and *cr-nfyc10* mutants (fig. S21, A to D). In agreement with this result, we observed that the expression levels of these genes are higher in the *cr-nas1*, *cr-nap1*, and *cr-nas1nap1-1* nodules than in wild-type nodules after sucrose treatment (Fig. 4C). Although several glycolytic genes were also down-regulated in sucrose-treated leaves of wild type, the down-regulation was unaffected in sucrose-treated leaves of *cr-nas1*, *cr-nap1*, and *cr-nas1nap1-1* (fig. S21E). Sucrose treatment also reduced PK2a protein content and PK activity in W82 nodules, but the decrease was eliminated in the *cr-nas1*, *cr-nap1*, and *cr-nas1nap1-1* nodules (fig. S21, F and G). Therefore, the pyruvate contents in the *cr-nas1*, *cr-nap1*, and *cr-nas1nap1-1* nodules were higher than that in wild-type nodules after sucrose treatment (Fig. 4D). Furthermore, we found that the 2-phosphoglycerate (2-PG) and phosphoenolpyruvate (PEP) contents were far lower than the pyruvate and oxaloacetic acid (OAA) contents in nodules (Fig. 4, D, E, G, and H), and expression of *ENO2a*, *ENO2b*, *ENO2c*, and *ENO2d* in the *GmNAS1* and *GmNAP1* mutants was similar to that in the wild type (Fig. 4F), suggesting that most of the 2-PG and PEP was converted into PEP, and pyruvate and OAA in nodules, respectively, and the total amount of PEP converted into pyruvate and OAA in W82 nodules should be similar to that in the *cr-nas1*, *cr-nap1* and *cr-nas1nap1-1* nodules. OAA

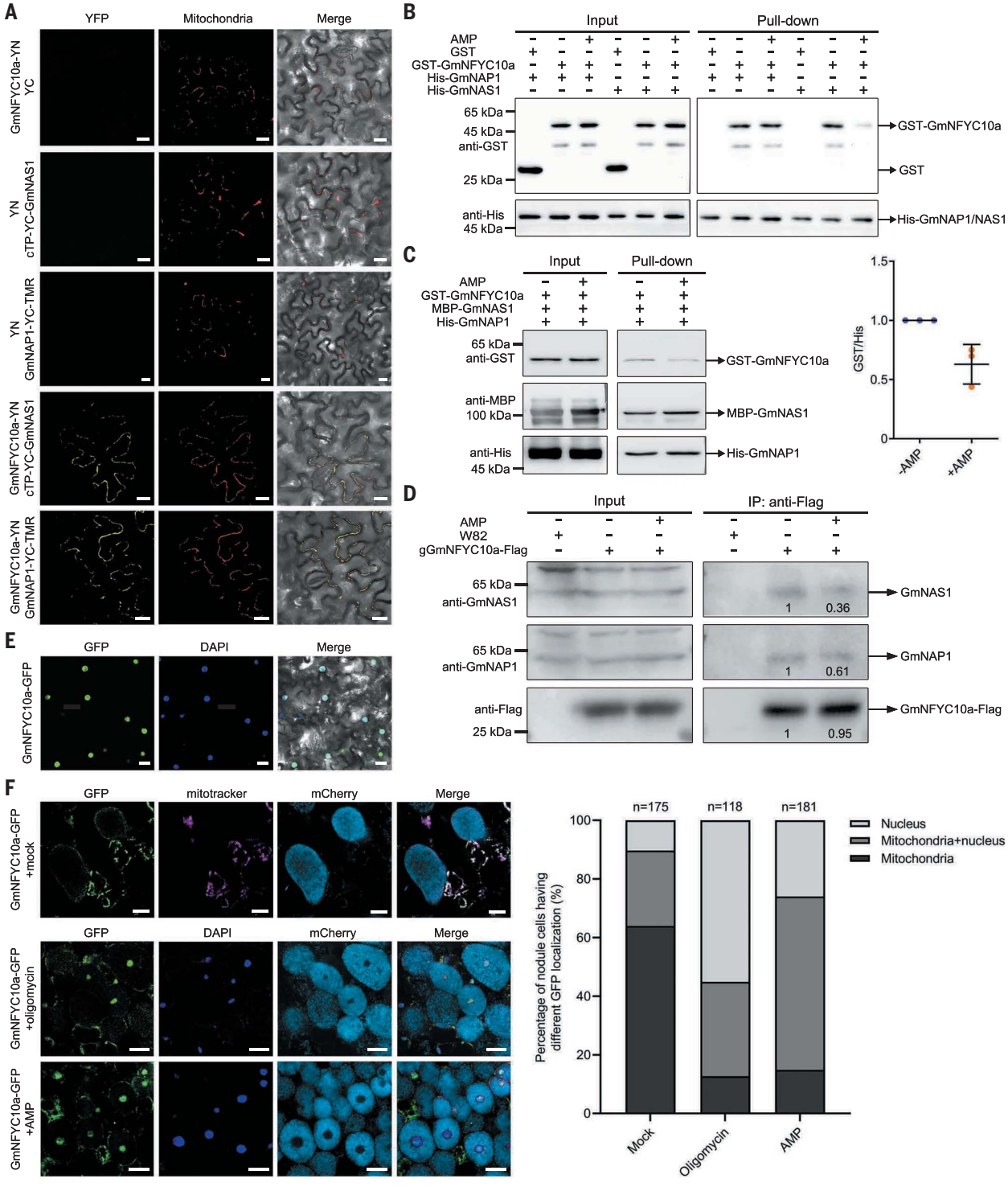

Fig. 2. GmNAS1 and GmNAP1 mediate GmNFYC10a nuclear accumulation in response to nodule energy state. (**A**) BiFC assays of GmNAS1 and GmNAP1 and GmNFYC10a. The mt-rk plasmid was co-infiltrated into *N. benthamiana* leaves to label mitochondria with mCherry fluorescence. YFP, yellow fluorescent protein. (**B**) Pull-down assays of GmNAS1 and GmNAP1 and GmNFYC10a. (**C**) Pull-down assay of GmNAP1 and GmNFYC10a in the presence of GmNAS1. The grayscale ratio of GST-GmNFYC10a to His-GmNAP1 (GST/His) with AMP was normalized to that without AMP; the result of three biological replicates is shown in the scatterplot to the right. (**D**) Co-IP assays of GmNAS1 and GmNAP1 and GmNFYC10a. The numbers under the lanes indicate relative band intensity quantified by ImageJ. (**E**) GmNFYC10a-GFP localization in *N. benthamiana* leaf epidermal cells. (**F**) GmNFYC10a-GFP localization in nodule cells. Nodules of *gGmNFYC10a-GFP* hairy roots were sectioned to observe GFP fluorescence. Mitotracker and 4′,6-diamidino-2-phenylindole (DAPI) were used to label mitochondria and nuclei, respectively; mCherry fluorescence indicates infected cells containing USDA110-mCherry. Nodule slices were treated with oligomycin or AMP to induce energy stress. In (B) to (D), AMP was added to a 0.5 mM final concentration, and the experiments were performed three times with comparable results. In (A), (E), and (F), scale bars are 20 μm.

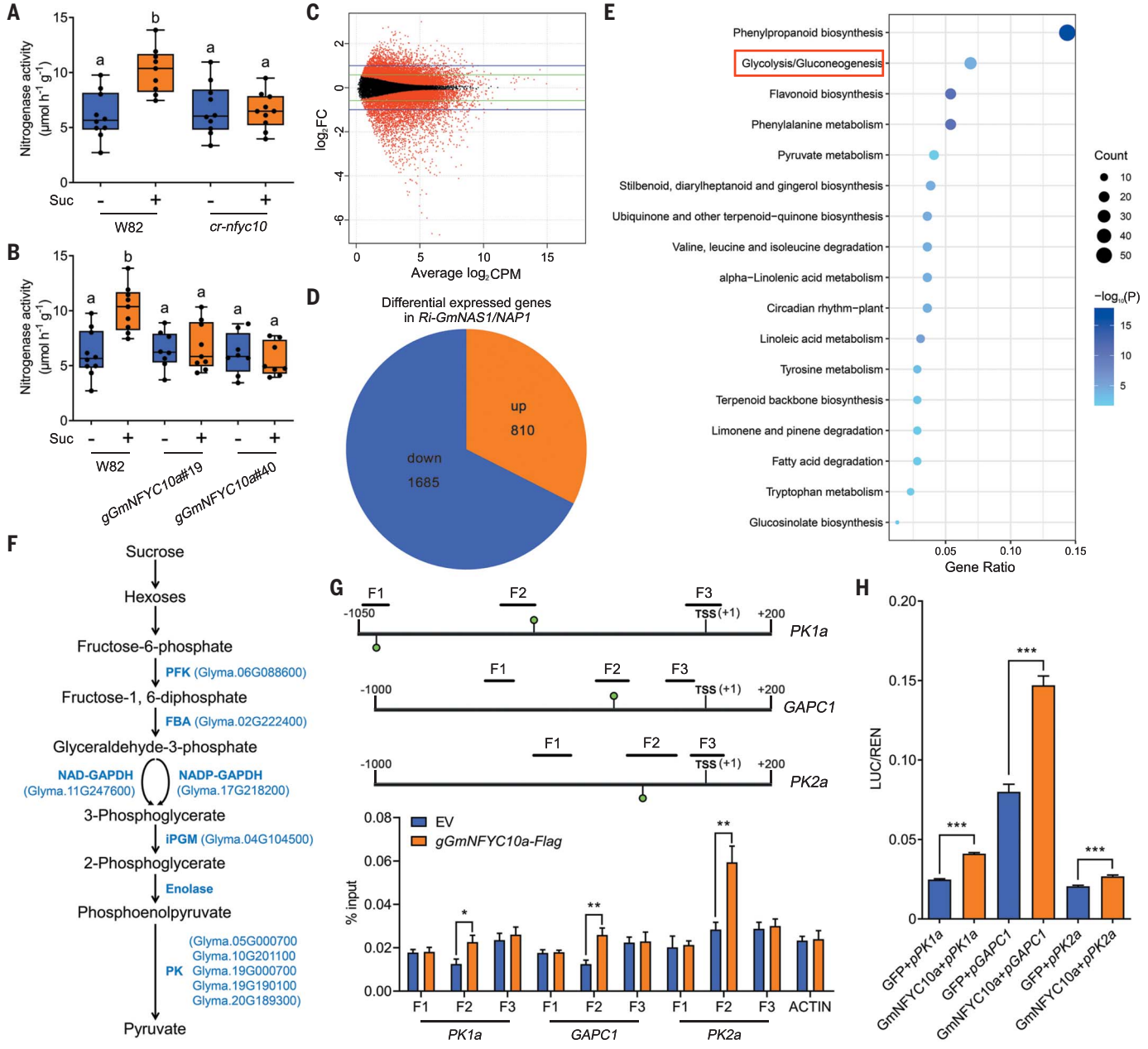

Fig. 3. GmNFYC10 regulates the response of nodule nitrogen fixation capacity to nodule energy state and the expression of glycolytic genes. (**A**) Nodule nitrogenase activity of W82 and *cr-nfyc10* without and with sucrose treatment. (**B**) Nodule nitrogenase activity of W82 and *gGmNFYC10a-Flag* transgenic lines without and with sucrose treatment. (**C**) Volcano plot of differentially expressed genes in empty vector (EV) and *Ri-GmNAS1-NAP1* hairy root nodules. CPM, counts per million; FC, fold change. (**D**) Differentially expressed genes (≥2-fold) in *Ri-GmNAS1-NAP1* nodules. (**E**) KEGG analysis of down-regulated genes (≥2-fold) in *Ri-GmNAS1-NAP1* nodules. The red frame indicates the glycolysis-gluconeogenesis pathway. (**F**) Schematic diagram of the glycolytic pathway. Ten down-regulated glycolytic genes in *Ri-GmNAS1-NAP1* nodules are indicated. FBA, fructose bisphosphate aldolase; GAPDH, glyceraldehyde phosphate dehydrogenase; iPGM, independent phosphoglycerate mutase; NAD, nicotinamide adenine dinucleotide; NADP, nicotinamide adenine dinucleotide phosphate; PFK, phosphofructokinase. (**G**) ChIP-qPCR (chromatin immunoprecipitation–quantitative polymerase chain reaction) analysis of GmNFYC10a binding to the *PK1a*, *GAPC1*, and *PK2a* promoters. NF-Y binding sites and DNA fragments for qPCR analysis are indicated by green circles and short horizontal lines, respectively. Data are means ± SD of three biological replicates. TSS, transcription start site. (**H**) Transcriptional activation of the *PK1a*, *GAPC1*, and *PK2a* promoters by GmNFYC10a. Firefly luciferase (LUC) activity was normalized to *Renilla* luciferase (REN) activity. Data are means ± SD of three biological replicates. Significant differences were determined by one-way ANOVA with post hoc Tukey's test ($P < 0.05$) in (A) and (B) or by Student's *t* test (*$P < 0.05$, **$P < 0.01$, and ***$P < 0.001$) in (G) and (H). In (A) and (B), boxes represent the first quartile, median, and third quartile, and whiskers represent minimum and maximum values.

and malate contents in these mutant nodules were lower (Fig. 4H), and the ratio of pyruvate to OAA in mutant nodules was increased (Fig. 4I). Moreover, under our growth conditions, the pyruvate, OAA, and malate contents in the *cr-nas1*, *cr-nap1*, and *cr-nas1nap1-1* nodules were similar to those in W82 nodules (fig. S21, H to J), which is in line with the unaffected nodule nitrogen fixation capacity of these mutants under the same growth conditions (Fig. 1H). Therefore, in response to an increased nodule energy state, GmNAS1 and GmNAP1

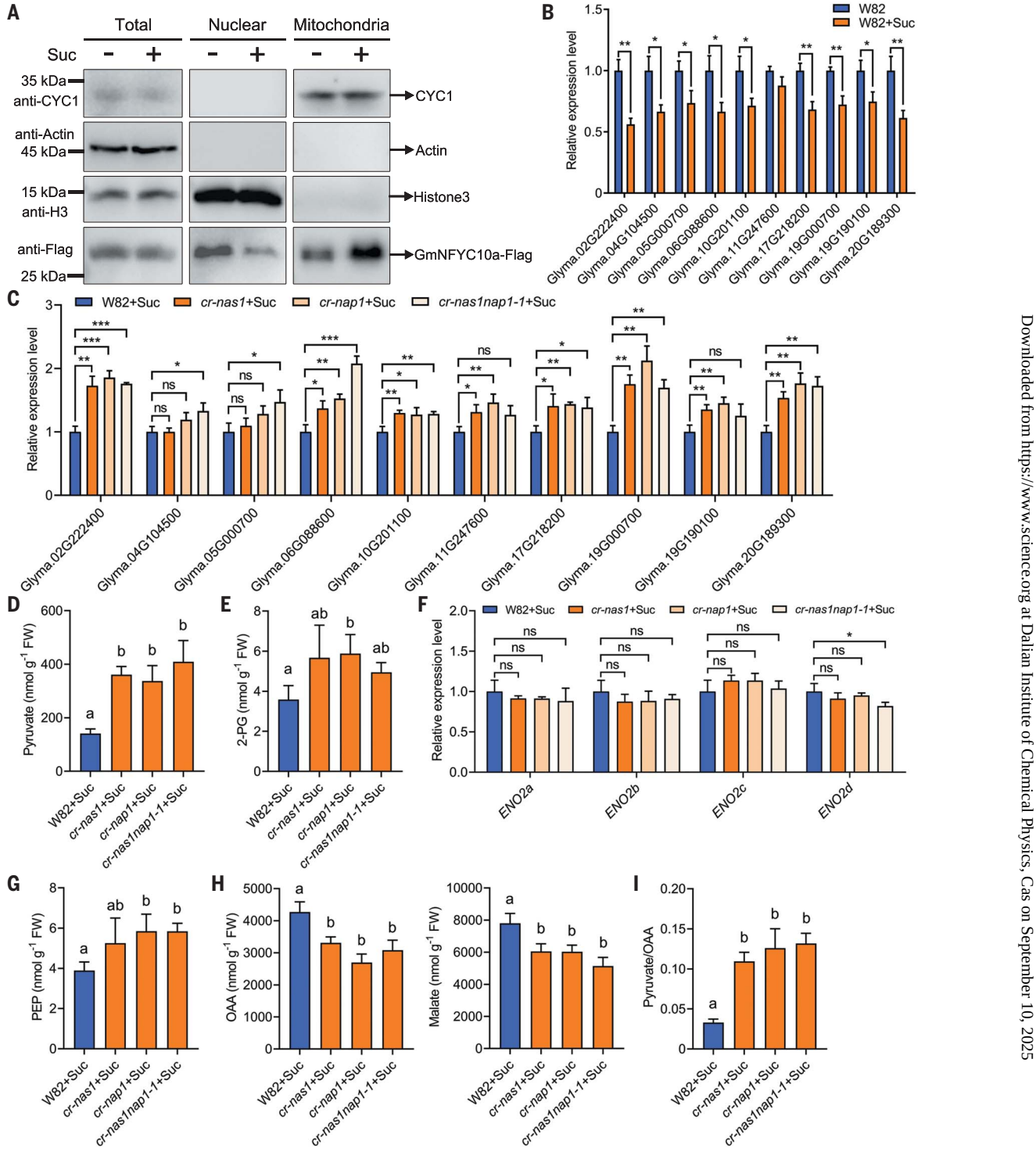

Fig. 4. GmNAS1, GmNAP1 and GmNFYC10 regulate glycolysis to modulate PEP allocation in response to nodule energy state. (**A**) GmNFYC10a-Flag protein abundance in the nucleus and mitochondria of nodule cells. CYC1, actin, and histone H3 were used as mitochondrial, cytoplasmic, and nuclear markers, respectively. The experiment was performed three times with comparable results. (**B**) Relative expression levels of glycolytic genes in W82 nodules without and with sucrose treatment. (**C**) Relative expression levels of glycolytic genes in W82, *cr-nas1*, *cr-nap1*, and *cr-nas1nap1-1* nodules after sucrose treatment. (**D** and **E**) Pyruvate (D) and 2-PG (E) contents in W82, *cr-nas1*, *cr-nap1*, and *cr-nas1nap1-1* nodules after sucrose treatment. (**F**) Relative expression levels of enolase genes *ENO2a*, *ENO2b*, *ENO2c*, and *ENO2d* in W82, *cr-nas1*, *cr-nap1*, and *cr-nas1nap1-1* nodules after sucrose treatment. (**G** to **I**) PEP (G), OAA (H), and malate (H) contents and ratio of pyruvate to OAA (I) in W82, *cr-nas1*, *cr-nap1*, and *cr-nas1nap1-1* nodules after sucrose treatment. Data in (D), (E), and (G) to (I) are means ± SD of at least four biological replicates. Significant differences were determined by Student's *t* test (*$P < 0.05$, **$P < 0.01$, and ***$P < 0.001$) in (B), (C), and (F) or by one-way ANOVA with post hoc Tukey's test ($P < 0.05$) in (D), (E), and (G) to (I); ns is not significant.

reduce GmNFYC10 nuclear accumulation, which suppresses glycolysis and pyruvate production, thereby modulating PEP allocation to favor nodule nitrogen fixation.

Discussion

Leguminous plants regulate high-energy-consuming symbiotic nitrogen fixation to optimize carbon utilization for sustaining growth under different environments (*32*). In this study, we identified GmNAS1 and GmNAP1 as nodule-specific energy sensors in soybean. Under our growth conditions, a limited sucrose supply keeps nodule cells in a relatively low-energy state with high AMP levels, which promotes the formation of GmNAS1-GmNAP1 heterodimers and leads to the nuclear accumulation of GmNFYC10, driving glycolysis and pyruvate production (fig. S22, A and B). Upon additional sucrose supply, when nodule energy state rises as AMP levels fall, GmNAS1 and GmNAP1 mainly form homodimers that maintain GmNFYC10 on mitochondria to reduce its nuclear accumulation, leading to lower pyruvate production and more PEP allocated to OAA (fig. S22, C and D). Thus, the ratio of PEP converted into pyruvate and OAA is largely dependent on nodule energy state in the wild type (36/64 at the low–nodule energy state versus 3/97 at the high–nodule energy state) to ensure basic cellular activities at the low–nodule energy state and to power nitrogen fixation at the high–nodule energy state (fig. S22, A and C). In the *cr-nas1nap1* mutant, enhanced allocation of PEP into OAA at the high-energy state was attenuated (pyruvate/OAA = 36/64 at the low–nodule energy state versus 12/88 at the high–nodule energy state) (fig. S22, B and D). Therefore, GmNAS1 and GmNAP1 are activated by the high-energy state under adequate carbohydrate supply to hold GmNFYC10a on the mitochondria, thereby enhancing PEP allocation to OAA and malate for nitrogen fixation, which is different from the canonical energy sensors AMPK, SNF1, and SnRK1 that are activated by the low-energy state in response to lack of nutrients (*22*, *33*, *34*). Although *GmNAS1* and *GmNAP1* knockouts did not affect nodule nitrogen fixation capacity under normal growth conditions (Fig. 1G), *GmNAS1* and *GmNAP1* knockdowns in hairy roots impaired nodule nitrogen fixation capacity (fig. S3). The nodule energy state of hairy roots is lower than that of normal plants (fig. S23A), which could be caused by the retarded plant growth of hairy roots (fig. S23B). The up-regulated genes in hairy root nodules showed that many stress-related pathways are activated (fig. S23, C to E), suggesting that *GmNAS1* and *GmNAP1* may also play a role in maintaining nodule nitrogen fixation capacity under stressful conditions. Phylogenetic analysis showed that GmNAS1 and GmNAP1 and their homologs within the ureide-exporting legumes form an independent cluster (fig. S24A and data S3) and that their homologs in *Phaseolus vulgaris*, but not in *Lotus japonicus* and *Medicago truncatula*, can complement the mutant nodule phenotypes of *cr-nas1* and *cr-nap1* (fig. S24B). Therefore, this set of energy sensors likely emerges in the ureide-exporting legumes to ensure elaborate energy use during nitrogen fixation, which may be necessary because of enhanced de novo purine biosynthesis and one-carbon metabolism in nodules of these legumes (*6*, *9*). Our findings show how legume nodule energy state modulates nodule performance through GmNAS1 and GmNAP1 and reveal targets for designing crops efficient in both carbon utilization, symbiotic nitrogen fixation, and growth under varying environmental conditions.

REFERENCES AND NOTES

1. J. G. Streeter, *Adv. Bot. Res.* **18**, 129–187 (1991).
2. C. Vance, in *Nitrogen-Fixing Leguminous Symbioses* (Springer, 2008), pp. 293–320.
3. M. Udvardi, P. S. Poole, *Annu. Rev. Plant Biol.* **64**, 781–805 (2013).
4. J. B. Peterson, H. J. Evans, *Plant Physiol.* **61**, 909–914 (1978).
5. J. B. Peterson, H. J. Evans, *Biochim. Biophys. Acta* **567**, 445–452 (1979).
6. K. R. Schubert, *Annu. Rev. Plant Physiol.* **37**, 539–574 (1986).
7. A. Millar, D. Day, F. Bergersen, *Plant Cell Environ.* **18**, 715–726 (1995).
8. C. A. Atkins, P. Smith, P. J. Storer, *Plant Physiol.* **113**, 127–135 (1997).
9. P. M. Smith, C. A. Atkins, *Plant Physiol.* **128**, 793–802 (2002).
10. S. Tajima, M. Nomura, H. Kouchi, *Front. Biosci.* **9**, 1374–1381 (2004).
11. T. M. Ching, *Life Sci.* **18**, 1071–1076 (1976).
12. T. M. Sa, D. W. Israel, *Plant Physiol.* **97**, 928–935 (1991).
13. T. M. Ching, S. Hedtke, S. A. Russell, H. J. Evans, *Plant Physiol.* **55**, 796–798 (1975).
14. Y. Kanayama, Y. Yamamoto, *Plant Cell Physiol.* **31**, 893–895 (1990).
15. A. J. Gordon, L. Skøt, C. L. James, F. R. Minchin, *J. Exp. Bot.* **53**, 423–428 (2002).
16. I. Lambert *et al.*, *J. Exp. Bot.* **71**, 5039–5052 (2020).
17. M. Janošík, V. Kery, M. Gaustadnes, K. N. Maclean, J. P. Kraus, *Biochemistry* **40**, 10625–10633 (2001).
18. B. Xiao *et al.*, *Nature* **449**, 496–500 (2007).
19. R. Townley, L. Shapiro, *Science* **315**, 1726–1729 (2007).
20. C. Hackenberg *et al.*, *Proc. Natl. Acad. Sci. U.S.A.* **115**, 7141–7146 (2018).
21. A. A. Baykov, H. K. Tuominen, R. Lahti, *ACS Chem. Biol.* **6**, 1156–1163 (2011).
22. D. G. Hardie, F. A. Ross, S. A. Hawley, *Nat. Rev. Mol. Cell Biol.* **13**, 251–262 (2012).
23. A. González, M. N. Hall, S. C. Lin, D. G. Hardie, *Cell Metab.* **31**, 472–492 (2020).
24. K. S. Yoo *et al.*, *Plant Cell* **23**, 3577–3594 (2011).
25. Q. Hao *et al.*, *Int. J. Mol. Sci.* **17**, 620 (2016).
26. M. Libault *et al.*, *Plant J.* **63**, 86–99 (2010).
27. O. Duncan *et al.*, *Plant Physiol.* **157**, 1093–1113 (2011).
28. M. E. Zanetti, F. A. Blanco, M. P. Beker, M. Battaglia, O. M. Aguilar, *Plant Cell* **22**, 4142–4157 (2010).
29. Q. Zhuang *et al.*, *Plant J.* **108**, 1422–1438 (2021).
30. M. Kanehisa, M. Furumichi, Y. Sato, M. Kawashima, M. Ishiguro-Watanabe, *Nucleic Acids Res.* 10.1093/nar/gkac963 (2022).
31. V. Nardone, A. Chaves-Sanjuan, M. Nardini, *Biochim. Biophys. Acta. Gene Regul. Mech.* **1860**, 571–580 (2017).
32. S. Sulieman, L.-S. P. Tran, *Legume Nitrogen Fixation in a Changing Environment: Achievements and Challenges* (Springer, 2015).
33. P. Crozet *et al.*, *Front. Plant Sci.* **5**, 190 (2014).
34. T. Broeckx, S. Hulsmans, F. Rolland, *J. Exp. Bot.* **67**, 6215–6252 (2016).

ACKNOWLEDGMENTS

We thank J. Zhang, C. Lan, and X. Li (Henan University) for assisting in the determination of pyruvate, OAA, malate, 2-PG, PEP, ATP, ADP, and AMP contents. **Funding:** This research was supported by grants from the National Key Research and Development Program (grant no. 2022YFA0912100 to X.W. and X.K.; grant no. 2018YFE0112100 to X.W.), the National Natural Science Foundation of China (grant no. 31870257 to X.W.), the Zhongyuan Scholar of Henan Province (grant no. 224000510001 to X.W.), the Outstanding Talents Fund of Henan University of China (grant no. CX3050A092004 to X.W.), and the Program for Innovative Research Team in University of Henan Province (grant no. 23IRTSTHN020 to X.W. and X.K.). **Author contributions:** X.K. and X.W. designed the experiments; X.K. performed most of the experiments; H.X. contributed to the vector construction, material collection, and nodulation assays; J.W., X.K., and X.W. analyzed RNA-seq data; Y.P. and Q.L. generated the stable transgenic soybean plants; and X.K. and X.W. wrote the manuscript. **Competing interests:** The authors declare no competing interests. **Data and materials availability:** RNA-seq data can be accessed through the National Center for Biotechnology Information (NCBI) (BioProject ID: PRJNA807470). All other data are available in the main text or supplementary materials. For material requests, please contact the corresponding author.

SUPPLEMENTARY MATERIALS

science.org/doi/10.1126/science.abq8591
Materials and Methods
Figs. S1 to S24
Table S1
References (*35*–*43*)
MDAR Reproducibility Checklist
Data S1 to S3

View/request a protocol for this paper from *Bio-protocol*.

Submitted 5 May 2022; resubmitted 10 October 2022
Accepted 8 November 2022
10.1126/science.abq8591